Journal of Inorganic Biochemistry 160 (2016) 94–105

Contents lists available at ScienceDirect

Journal of Inorganic Biochemistry

journal homepage: www.elsevier.com/locate/jinorgbio

Synthesis, characterization and biological evaluation of ^{99m}Tc/Re–tricarbonyl quinolone complexes

Theocharis E. Kydonaki [a,b], Evangelos Tsoukas [c], Filipa Mendes [d], Antonios G. Hatzidimitriou [a], António Paulo [d], Lefkothea C. Papadopoulou [c], Dionysia Papagiannopoulou [b,*], George Psomas [a,*]

[a] Department of General and Inorganic Chemistry, Faculty of Chemistry, Aristotle University of Thessaloniki, GR-54124 Thessaloniki, Greece
[b] Department of Pharmaceutical Chemistry, School of Pharmacy, Aristotle University of Thessaloniki, GR-54124 Thessaloniki, Greece
[c] Department of Pharmacognosy - Pharmacology, School of Pharmacy, Aristotle University of Thessaloniki, GR-54124 Thessaloniki, Greece
[d] Centro de Ciências e Tecnologias Nucleares (C^{2}TN), Instituto Superior Técnico, Universidade de Lisboa, Campus Tecnológico e Nuclear, Estrada Nacional 10, 2695-066 Bobadela LRS, Portugal

ARTICLE INFO

Article history:
Received 1 October 2015
Received in revised form 26 November 2015
Accepted 16 December 2015
Available online 21 December 2015

Keywords:
Quinolones
Rhenium complexes
Technetium-99m
Imaging agents
Biological activity

ABSTRACT

New rhenium(I) tricarbonyl complexes with the quinolone antimicrobial agents oxolinic acid (Hoxo) and enrofloxacin (Herx) and containing methanol, triphenylphosphine (PPh_3) or imidazole (im) as unidentate co-ligands, were synthesized and characterized. The crystal structure of complex $[Re(CO)_3(oxo)(PPh_3)]\cdot 0.5MeOH$ was determined by X–ray crystallography. The deprotonated quinolone ligands are bound bidentately to rhenium(I) ion through the pyridone oxygen and a carboxylate oxygen. The binding of the rhenium complexes to calf-thymus DNA (CT DNA) was monitored by UV spectroscopy, viscosity measurements and competitive studies with ethidium bromide; intercalation was suggested as the most possible mode and the DNA-binding constants of the complexes were calculated. The rhenium complex $[Re(CO)_3(erx)(im)]$ was assayed for its topoisomerase IIα inhibition activity and was found to be active at 100 μM concentration. The interaction of the rhenium complexes with human or bovine serum albumin was investigated by fluorescence emission spectroscopy (through the tryptophan quenching) and the corresponding binding constants were determined. The tracer complex $[^{99m}Tc(CO)_3(erx)(im)]$ was synthesized and identified by comparative HPLC analysis with the rhenium analog. The ^{99m}Tc complex was found to be stable in solution. Upon injection in healthy mice, fast tissue clearance of the ^{99m}Tc complex was observed, while both renal and hepatobiliary excretion took place. Preliminary studies in human K-562 erythroleukemia cells showed cellular uptake of the ^{99m}Tc tracer with distribution primarily in the cytoplasm and the mitochondria and less in the nucleus. These preliminary results indicate that the quinolone ^{99m}Tc/Re complexes show promise to be further evaluated as imaging or therapeutic agents.

1. Introduction

Quinolones are synthetic antibacterial drugs used for the treatment of diverse infections such as urinary tract, respiratory and bone–joint infections, sexually transmitted diseases, prostatitis, pneumonia and acute bronchitis [1–3]. Since quinolones inhibit the activity of the enzyme DNA-topoisomerase II which is essential for the replication and transcription of DNA [4,5], their interaction with various types of DNA has been also studied in addition to their antibacterial activity on diverse microorganisms [6]. Due to the homology of bacterial topoisomerases to the mammalian ones, some quinolone derivatives have also been shown to inhibit mammalian type II topoisomerase, leading to cytotoxicity. Therefore, these quinolone derivatives are attractive lead compounds for the development of antineoplastic topoisomerase inhibitors [7–10]. Furthermore, in comparison to free quinolones, their metal complexes [3,11] have shown enhanced binding affinity to DNA [12–14] and serum albumins [15–18], increased antibacterial activity [19–22], and, in some cases, noteworthy antiproliferative activity [23,24].

Oxolinic acid (Hoxo, Fig. 1(A)) is a first-generation quinolone [2,3] which has been used for the treatment of urinary tract infections for almost five decades [25]. Despite its long-time clinical use, only Cu(II) [26], Zn(II) [27,28], Ni(II) [16], Mn(II) [29] and Co(II) [30] complexes of oxolinic acid have been described and the crystal structures of only seven complexes have been structurally reported [11]. Enrofloxacin (Herx, Fig. 1(B)) is a second-generation quinolone with a broader spectrum of activity than Hoxo and is potent against a wide range of Gram-negative and Gram-positive bacteria [2,3]. Herx is often used for the treatment of urinary tract, respiratory tract and skin infectious diseases in pets and livestock [31]. A plethora of enrofloxacin complexes have been reported with Mn(II) [29], Fe(III) [32], Co(II) [22], Ni(II) [17], Zn(II) [18,33], Cu(II) [34,35], Cd(II) [36], Pb(II) [36], La(III) and Sm(II) [15].

* Corresponding authors.
E-mail addresses: papagd@pharm.auth.gr (D. Papagiannopoulou), gepsomas@chem.auth.gr (G. Psomas).

http://dx.doi.org/10.1016/j.jinorgbio.2015.12.010
0162-0134/

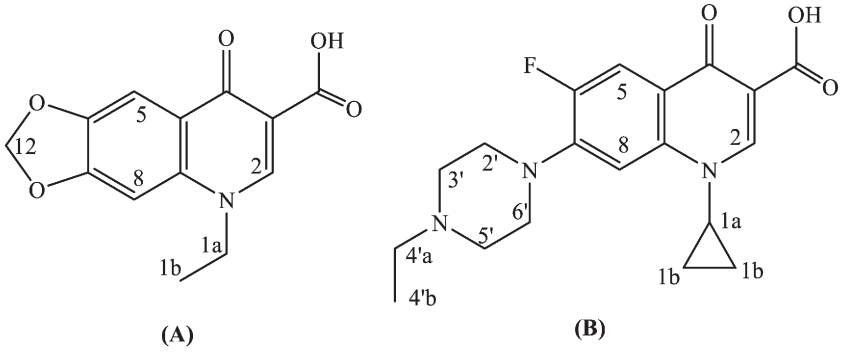

Fig. 1. The syntax formula of (A) oxolinic acid (Hoxo) and (B) enrofloxacin (Herx) and H atoms labeling.

Technetium-99m (^{99m}Tc) is an important radionuclide with wide applications in diagnostic Nuclear Medicine. It emits gamma radiation ($E_\gamma = 141$ keV) via isomeric transition with a half-life of 6 h, both ideal properties for use in Single Photon Emission Computed Tomography (S.P.E.C.T.). ^{99m}Tc radiopharmaceuticals are used routinely for the diagnosis of various medical conditions, by imaging organ function (myocardial/brain perfusion, etc.) or by targeting specific biological structures (cells, receptors) involved in disease [37,38]. Current radiopharmaceutical research is focused to a great extent on targeting cellular components that modulate important functions, like cell-membrane receptors [39,40], mitochondria [41,42] or DNA [43,44] in an effort to efficiently diagnose and treat cancer, infection and other conditions.

In the past few years, the development of new targeted imaging agents of ^{99m}Tc has focused a lot on the low oxidation state ^{99m}Tc-tricarbonyl core, *fac*-$[^{99m}Tc(CO)_3]^+$ due to its high biological stability and its versatility in ligand selection [45]. Labeling strategies with the ^{99m}Tc-tricarbonyl core involve the use of tridentate chelators or the combination of a bidentate chelating and a monodentate ligand, the latter known as [2 + 1] approach [46]. Efforts to develop radiotracers based on the ^{99m}Tc-tricarbonyl core in order to target nuclear DNA for imaging or radiotherapy of cancer have also emerged. In these efforts, acridine orange, anthracene or pyrene intercalators were conjugated on the radiometal via suitable chelators [43,44,47–49].

Quinolones radiolabeled with ^{99m}Tc have also been investigated as infection specific imaging agents; in particular ciprofloxacin has been radiolabeled with ^{99m}Tc either by direct labeling [50] or by the organometallic ^{99m}Tc-tricarbonyl core [51,52].

Rhenium complexes are oftentimes used as non-radioactive analogs of technetium-99m tracers. Nevertheless, there is a growing body of evidence that rhenium complexes and in particular $[Re(CO)_3]$ complexes possess significant cytotoxic properties [53]. The majority of these compounds contain polypyridine or bis(quinoline) ligands and are fluorescent, exhibiting thus phototoxicity [54,55]. In addition, a number of Re complexes exhibit "standard" cytotoxicity [53]. Also, a number of these compounds accumulate in the mitochondria due to their cationic and lipophilic nature [56].

In the present manuscript, the interaction of oxolinic acid and enrofloxacin with rhenium(I) is investigated in the presence of methanol, triphenylphosphine (PPh_3) or imidazole (im) as co-ligands. The rhenium(I) tricarbonyl complexes $[Re(CO)_3(oxo)(MeOH)]$, **Re1,** $[Re(CO)_3(erx)(MeOH)]$, **Re2,** $[Re(CO)_3(oxo)(PPh_3)]\cdot0.5MeOH$, **Re3,** $[Re(CO)_3(erx)(PPh_3)]$, **Re4** and $[Re(CO)_3(erx)(im)]$, **Re5,** were prepared and characterized by physicochemical and spectroscopic techniques. The crystal structure of complex $[Re(CO)_3(oxo)(PPh_3)]\cdot0.5MeOH$, **Re3** was determined by X-ray crystallography. Additionally, the biological properties of the rhenium complexes were evaluated in regard to their interaction with calf-thymus (CT) DNA as investigated by UV spectroscopy, viscosity measurements and competitive studies with the classical DNA-intercalator ethidium bromide (EB) monitored by fluorescence emission spectroscopy. Moreover, their affinity to bovine (BSA) and human (HSA) serum albumins was investigated by fluorescence emission spectroscopy. Investigation of potential topoisomerase IIα enzyme inhibition of the selected quinolone Re-tricarbonyl complex, **Re5**, was also conducted. The radiotracer complex $[^{99m}Tc(CO)_3(erx)(im)]$ was prepared, in order to investigate its uptake in cancer cells, and in addition its biodistribution in healthy mice was evaluated after intravenous administration.

2. Experimental

2.1. Materials – instrumentation – physical measurements

All the chemicals were purchased from Sigma-Aldrich Co and all solvents were purchased from ChemLab. They were of reagent grade and were used as purchased unless otherwise noted. $[NEt_4]_2[ReBr_3(CO)_3]$ was prepared from Re_2CO_{10} according to the literature [57]. $[Re(CO)_5(O_3SCF_3)]$ was converted to $[Re(CO)_3(H_2O)_3](OCF_3)$ as described in the literature [58]. Precursor *fac*-$[^{99m}Tc(CO)_3(H_2O)_3]^+$ was prepared by a standard method where 1 mL of $[^{99m}TcO_4^-]$ ^{99}Mo/^{99m}Tc generator eluate was added to a kit containing 5.5 mg $NaBH_4$, 4 mg Na_2CO_3 and 15 mg Na–K tartrate, purged with CO gas and the mixture was heated in boiling water for 30 min [59].

DNA stock solution was prepared by dilution of CT DNA to buffer (containing 15 mM trisodium citrate and 150 mM NaCl at pH 7.0) followed by exhaustive stirring for three days, and kept at 4 °C for no longer than a week. The stock solution of CT DNA gave a ratio of UV absorbance at 260 and 280 nm (A_{260}/A_{280}) of 1.85, indicating that the DNA was sufficiently free of protein contamination [60]. The DNA concentration was determined by the UV absorbance at 260 nm after 1:20 dilution using $\varepsilon = 6600\ M^{-1}\ cm^{-1}$ [61].

IR spectra were recorded as KBr pellets on a Perkin–Elmer FT–IR Spectrum BX spectrophotometer in the region 500–4000 cm^{-1}. UV–visible (UV–vis) spectra were recorded as nujol mulls and in solution at concentrations in the range 10^{-5}–5×10^{-3} M on a Hitachi U-2001 dual beam spectrophotometer. ^{1}H–NMR spectra of the rhenium complexes in DMSO-d_6 were recorded on an Agilent DD2 500 MHz spectrometer. C, H and N elemental analysis were performed on a Perkin-Elmer 240B elemental analyzer. Molar conductivity measurements were carried out with a Crison Basic 30 conductometer. Fluorescence spectra were recorded in solution on a Hitachi F-7000 fluorescence spectrophotometer. Viscosity experiments were carried out using an ALPHA L Fungilab rotational viscometer equipped with an 18 mL LCP spindle and the measurements were performed at 100 rpm. HPLC analysis was performed on an Agilent HP 1100 series pump, connected to a Gabi gamma detector (Raytest) and to an HP 1100 multiple wavelength detector. Separations were achieved on an Agilent Eclipse XDB-C18 column (25 cm × 4.6 mm, 5 μm) eluted with a binary gradient system of solvent A: 0.1% TFA in water and solvent B: methanol at 1 mL/min flow rate. Initial composition consisted of 100% A–0% B that linearly converted to 25% A–75% B over 15 min and

to 5% A–95% B from 15 to 20 min. The composition remained constant from 20 to 25 min at 95% B.

2.2. Synthesis of the rhenium–quinolone complexes

2.2.1. Synthesis of $[Re(CO)_3(Q)(MeOH)]$, **Re1** and **Re2** (Q = oxo for **Re1** and erx for **Re2**)

$[NEt_4]_2[ReBr_3(CO)_3]$ (38 mg, 0.05 mmol) was dissolved in water (1 mL), $AgNO_3$ (25 mg, 0.15 mmol) was added and the mixture was stirred for 15 min, in order to achieve precipitation of AgBr. After filtering the salt, water was evaporated and the rhenium precursor was redissolved in methanol (1 mL). To this solution of the precursor $[Re(CO)_3(MeOH)_3](NO_3)$, a solution of the quinolone [Hoxo (13 mg, 0.05 mmol) or Herx (18 mg, 0.05 mmol)] with KOH/MeOH 1 M (50 μL) in methanol (4 mL) was added and the reaction mixture was refluxed for 2.5 h, after which a white residue was formed. The solid was filtered and washed with water and methanol.

*2.2.1.1. $[Re(CO)_3(oxo)(MeOH)]$, **Re1**:* Yield: 14 mg (50%). HPLC retention time (t_R): 18.1 min. Anal. Calc. for $C_{17}H_{15}NO_9Re$ (MW = 563.51) C 36.24, H: 2.68, N: 2.49; found: C: 36.66, H: 2.82, N: 2.31. IR (cm^{-1}, KBr): 2014, 1888, 1860, 1644, 1603, 1466, 1400, 1266, 1038, 778. UV–vis in DMSO; λ, nm (ε, M^{-1} cm^{-1}): 338 (12,000), 307 (14,400). ^{1}H-NMR (500 MHz, DMSO-d_6) δ 9.03 (s, 1H, H2), 7.66 (s, 1H, H5), 7.60 (s, 1H, H8), 6.30 (d, J = 4.7 Hz, 2H, H12), 4.57 (q, 2H, H1a), 1.37 (t, 3H, H1b). The complex is soluble in DMSO (molar conductivity, Λ_M = 9 S cm^2 mol^{-1}, in 1 mM DMSO solution).

*2.2.1.2. $[Re(CO)_3(erx)(MeOH)]$, **Re2**:* Yield: 9 mg (27%). t_R: 16.3 min. Anal. Calc. for $C_{23}H_{25}FN_5O_7Re$ (MW = 660.67) C: 41.81, H: 3.81, N: 6.36; found: C: 42.18, H: 4.04, N: 6.44. IR (cm^{-1}, KBr): 2019, 1896, 1875, 1615, 1610, 1482, 1379, 1256. UV–vis in DMSO; λ, nm (ε, M^{-1} cm^{-1}): 343 (13,700), 280 (22,000). ^{1}H-NMR (500 MHz, DMSO-d_6) δ 8.87 (s, 1H, H2), 7.87 (d, J = 13.4 Hz, 1H, H5), 7.55 (d, J = 7.4 Hz, 1H, H8), 3.86 (m, 1H, H1a), ~3.3 (m, 4H, 2′, 6′),[1] 2.57 (m, 4H, 3′, 5′), 2.40 (q, 2H, H4a′), 1.33 (m, 2H, H1b), 1.20 (m, 1H, H1b), 1.11 (m, 1H, H1b), 1.03 (t, 3H, H4b′). The complex is soluble in ethanol, methanol, dichloromethane and DMSO (Λ_M = 5 S cm^2 mol^{-1}, in 1 mM DMSO solution).

2.2.2. Synthesis of complexes $[Re(CO)_3(Q)(PPh_3)]$, **Re3** and **Re4** (Q = oxo for **Re3** and erx for **Re4**)

To a solution of $[Re(CO)_3(MeOH)_3](NO_3)$ (0.05 mmol), prepared as described above, a solution of the quinolone [Hoxo (13 mg, 0.05 mmol) or Herx (18 mg, 0.05 mmol)] with KOH/MeOH 1 M (50 μL) and triphenylphosphine (PPh_3) (13 mg, 0.05 mmol) in methanol (4 mL) was added, and the reaction mixture was refluxed for 2.5 h. The yellow residue formed during the reaction was collected with filtration.

*2.2.2.1. $[Re(CO)_3(oxo)(PPh_3)]$·0.5MeOH, **Re3**:* Upon re-crystallization from methanol, yellow crystals (11 mg, 28%) suitable for X-ray structure determination were obtained. t_R: 22.5 min. Anal. Calc. for $C_{34.5}H_{27}N_1O_{8.5}P_1Re_1$ (MW = 808.77) C 51.24, H: 3.36, N: 1.73; found: C: 50.96, H: 3.56, N: 2.03. IR (cm^{-1}, KBr): 2021, 1911, 1885, 1638, 1605, 1471, 1385, 1264, 1036, 748, 695. UV–vis in DMSO; λ, nm (ε, M^{-1} cm^{-1}): 344 (11,000). ^{1}H–NMR (500 MHz, DMSO-d_6) δ 8.58 (s, 1H, H2), 7.52 (s, 1H, H5), 7.44 (s, 1H, H8), 7.41–7.26 (m, 12H, H_{Ph}), 7.22 (m, 3H, H_{Ph}) 6.29 (d, J = 4.7 Hz, 2H, H12), 4.39 (q, 2H, H1a), 1.28 (t, 3H, H1b). The complex is soluble in CH_2Cl_2 and DMSO (Λ_M = 12 S cm^2 mol^{-1}, in 1 mM DMSO solution).

[1] Peak hiding under the H_2O solvent peak.

*2.2.2.2. $[Re(CO)_3(erx)(PPh_3)]$, **Re4**:* Re-crystallization from dichloromethane–hexane, 1:1. Yield: 21 mg (47%). t_R: 20.5 min. Anal. Calc. for $C_{40}H_{36}FN_3O_6PRe$ (MW = 890.92) C 53.93, H: 4.07, N: 4.72; found: C: 53.66, H: 3.82, N: 4.35. IR (cm^{-1}, KBr): 2021, 1918, 1889, 1624, 1618, 1482, 1379, 1256, 747, 695. UV–vis in DMSO; λ, nm (ε, M^{-1} cm^{-1}): 342 (13,000), 283 (23,500). ^{1}H-NMR (500 MHz, DMSO-d_6) δ 8.43 (s, 1H, H2), 7.72 (d, J = 13.4 Hz, 1H, H5), 7.42 (d, J = 7.4 Hz, 1H, H8), 7.39–7.29 (m, 12H, H_{Ph}), 7.22 (m, 3H, H_{Ph}), 3.72 (m, 1H, H1a), ~3.3 (m, 4H, 2′, 6′)[1], 2.60 (m, 4H, 3′, 5′), 1.25 (m, 4H, H1b), 1.03 (t, 3H, H4b′). The complex is soluble in methanol, CH_2Cl_2 and DMSO (Λ_M = 10 S cm^2 mol^{-1}, in 1 mM DMSO solution).

2.2.3. Synthesis of $[Re(CO)_3(erx)(im)]$, **Re5**

A methanolic solution (5 mL) of enrofloxacin (18 mg, 0.05 mmol), imidazole (3 mg, 0.05 mmol) and KOH/MeOH 1 M (50 μL) was added to an aqueous solution (5 mL) of $[Re(CO)_3(H_2O)_3](O_3SCF_3)$ (0.05 mmol) and the reaction mixture was refluxed for 3 h, afterwards a yellow residue was formed, filtered and washed with water. Yield: 16 mg (46%). t_R: 17.0 min. Anal. Calc. for $C_{25}H_{25}FN_5O_6Re$ (MW = 696.711) C: 43.10, H: 3.62, N: 10.05; found: C: 43.28, H: 3.74, N: 9.84. IR (cm^{-1}, KBr): 2017, 2000, 1880, 1629, 1618, 1481, 1381, 1257, 830, 750, 659. UV–vis in DMSO; λ, nm (ε, M^{-1} cm^{-1}): 342 (8500), 279 (16,100). ^{1}H-NMR (500 MHz, DMSO-d_6) δ 12.84 (s, 1H, N–H), 8.89 (s, 1H, H2), 8.01 (h, 1H, H2″), 7.93 (d, J = 13.4 Hz, 1H, H5), 7.53 (d, J = 7.4 Hz, 1H, H8), 7.19 (s, 1H, H5″), 6.99 (s, 1H, H4″), 3.82(m, 1H, H1a), ~3.3 (m, 4H, 2′, 6′) [1], 2.74 (m, 4H, 3′, 5′), 1.29 (m, 2H, H1b), 1.5 (m, 2H, H1b), 1.03 (t, 3H, H4b′). The complex is soluble in DMSO (Λ_M = 7 S cm^2 mol^{-1}, in 1 mM DMSO solution).

2.3. X-ray crystallography

Crystals of **Re3** were taken from the mother liquor and mounted at room temperature on a Bruker Kappa APEX2 diffractometer equipped with a triumph monochromator using Mo Kα radiation. Unit cell dimensions were determined and refined by using the angular settings of at least 100 high intensity reflections (>10 σ(I)) in the range $15 < 2\theta < 40°$. Intensity data were recorded using φ and ω scans. Crystal presented no decay during the data collection. The frames collected were integrated with the Bruker SAINT software package [62], using a narrow-frame algorithm. Data were corrected for absorption using the numerical method (SADABS) based on crystal dimensions [63]. The structure was solved using the SUPERFLIP package [64], incorporated in Crystals. Data refinement (full-matrix least-squares methods on F^2)

Table 1
Crystallographic data for complex **Re3**.

	Re3
Formula	$C_{34.50}H_{27}N_1O_{8.50}P_1Re_1$
F_w	808.77
T (K)=	295
Crystal system	Triclinic
Space group	P–1
a (Å)=	10.6921(6)
b (Å)=	11.8779(7)
c (Å)=	12.9937(7)
α (°)=	95.327(2)
β (°)=	97.805(2)
γ (°)=	93.164(2)
Volume ($Å^3$)=	1624.00(16)
Z	2
$d_{(calc)}$, Mg m^{-3}	1.65
Abs. coef., μ, mm^{-1}	3.845
F(000)	798
GOF on F^2	1.000
range of h, k, l	−13 → 10, −14 → 14, −15 → 16
Reflections, total/(with I > 2σ(I))	6686/5444
R1/wR2 (total)	0.0542/0.0940
R1/wR2 (with I > 2σ(I))	0.0365/0.0835

and all subsequent calculations were carried out using the Crystals version 14.61 program package [65].

All non-hydrogen atoms were refined anisotropically (even them from the disordered from the methanol solvent). Hydrogen atoms were located by difference maps at their expected positions and refined using soft constraints. By the end of the refinement, they were positioned geometrically using riding constraints to bonded atoms. Crystal data as well as details of data collection and structure refinement for the compounds are given in Table 1. Illustrations were drawn by CAMERON [66]. Further details on the crystallographic study as well as atomic displacement parameters are given as Supporting Information in the form of cif file.

2.4. Biological evaluation of the rhenium–quinolone

2.4.1. DNA-binding studies

2.4.1.1. Study with UV spectroscopy. The interaction of rhenium complexes with CT DNA was studied by UV spectroscopy in order to investigate the possible binding modes to CT DNA and to calculate the binding constants to CT DNA (K_b). The UV spectra of CT DNA were recorded for a constant DNA concentration in the presence of each compound at diverse [complex]/[DNA] mixing ratios ($=r$). The binding constant of the complexes with DNA, K_b (in M^{-1}), was determined by the Wolfe–Shimer equation (Eq. S1) [67] and the plots $^{[DNA]}/_{(\varepsilon_A-\varepsilon_f)}$ vs [DNA] using the UV spectra of the compound recorded for a constant concentration in the presence of DNA for diverse *r* values. Control experiments with DMSO were performed and no changes in the spectra of CT DNA were observed.

2.4.1.2. Viscometry. The viscosity of DNA ([DNA] = 0.1 mM) in buffer solution (150 mM NaCl and 15 mM trisodium citrate at pH 7.0) was measured in the presence of increasing amounts of the complexes (up to the value of r = 0.26). All measurements were performed at room temperature. The obtained data are presented as $(\eta/\eta_0)^{1/3}$ versus *r*, where η is the viscosity of DNA in the presence of the compound, and η_0 is the viscosity of DNA alone in buffer solution.

2.4.1.3. EB competitive studies with fluorescence spectroscopy. The competitive studies of the complexes with EB were investigated by fluorescence emission spectroscopy in order to examine whether the complexes can displace EB from its DNA–EB complex. The DNA–EB complex was prepared by adding 20 μM EB and 26 μM CT DNA in buffer (150 mM NaCl and 15 mM trisodium citrate at pH 7.0). The possible intercalating effect of the complexes was studied by adding a certain amount of a solution of the compound step by step into a solution of the DNA–EB complex. The influence of the addition of each complex to the DNA–EB complex solution was obtained by recording the changes of fluorescence emission spectra with excitation wavelength at 540 nm. The complexes did not show any appreciable fluorescence at room temperature in solution or in the presence of DNA under the same experimental conditions; therefore, the observed quenching is attributed to the displacement of EB from its EB–DNA complex. The values of the Stern–Volmer constant (K_{SV}, in M^{-1}) have been calculated according to the linear Stern–Volmer equation (Eq. S2) [68] and the plots $^{I_o}/_{I}$ vs [Q].

2.4.2. Albumin binding studies

The albumin binding study was performed by tryptophan fluorescence quenching experiments using bovine (BSA, 3 μM) or human serum albumin (HSA, 3 μM) in buffer (containing 15 mM trisodium citrate and 150 mM NaCl at pH 7.0). The quenching of the emission intensity of tryptophan residues of BSA at 343 nm or HSA at 351 nm was monitored using complexes **Re1–Re5** as quenchers with increasing concentration [69]. Fluorescence emission spectra were recorded in the range 300–500 nm at an excitation wavelength of 295 nm. The fluorescence emission spectra of the free complexes were also recorded under the same experimental conditions, i.e. excitation at 295 nm; for the enrofloxacinato complexes [22] a low-intensity maximum emission band appeared at 416 nm and for the oxolinato complexes [28] such band was observed at 372 nm. Therefore, the quantitative studies of the SA fluorescence spectra were performed after their correction by subtracting the spectra of the complexes.

The influence of the inner-filter effect [70] on the measurements was evaluated by Eq. S3. The Stern–Volmer and Scatchard equations (Eq. S4–S6) [71] and graphs have been used in order to study the interaction of each quencher with serum albumins and calculate the dynamic quenching constant K_{SV} (in M^{-1}), the quenching constant k_q (in $M^{-1}\,s^{-1}$), the SA-binding constant K (in M^{-1}) and the number of binding sites per albumin n.

2.4.3. Topoisomerase IIα inhibition

Topoisomerase inhibition capacity of the compounds was determined via a plasmid DNA relaxation assay, performed with Human Topoisomerase IIα from TopoGen Inc. (Buena Vista, CO, USA) according to manufacturer's instructions.

The supercoiled plasmid DNA ϕX174 (Promega) was used as a substrate and incubated with Topo IIα in the presence of compounds (fresh stock solutions prepared in DMSO). Typically, each reaction mixture was prepared by adding 2 μL (200 ng) of supercoiled DNA, 4 μL of topoisomerase reaction buffer, compound solution (ranging from 10 to 100 μM), 1 μL of Topo IIα (10 U/μL) and H_2O to a final volume of 20 μL. Etoposide at 1 mM was used as a positive control of inhibition. DMSO in the final reaction volume did not exceed 0.5%, and a sample with that concentration of DMSO was also included in the assay. The reaction mixture was incubated for 30 min at 37 °C. The reaction was stopped by the addition of 10% SDS followed by digestion with proteinase K for 15 min at 37 °C (Sigma). Linear DNA was obtained by digestion with the single-cutter restriction enzyme Xho I and used as a reference.

After incubation, DNA loading buffer was added and the sample loaded onto a 1% agarose gel in TAE buffer. The electrophoresis was carried out for 4 h at 50 V. The gels were then stained with TAE buffer containing GelRed (Biotium, Hayward, CA,USA). Bands were visualized under UV light and images captured using an AlphaImager EP (Alpha Innotech). Results are displayed in Fig. 7.

2.5. Radiochemistry

2.5.1. Synthesis of $[^{99m}Tc(CO)_3(erx)(im)]$

The precursor $[^{99m}Tc(CO)_3(H_2O)_3]^{+1}$ (5 m Ci/185 MBq, 0.5 mL) (pH 6) was added via syringe to a crimped vial with Herx (2 mg in 0.1 mL MeOH) and the mixture was heated at 95 °C for 30 min. Then, a solution of imidazole (1 mg in 0.1 mL MeOH) was added to the labeling mixture and additional heating at 95 °C followed for 45 min. The complex formation was verified by HPLC. Radiochemical yield: 73%. t_R: 17.1 min.

2.5.2. Stability

The HPLC-purified ^{99m}Tc complex (50 μL, approx. 10 MBq) was incubated with 0.5 mL of 0.1 M PBS pH 7.4, with and without addition of Herx (2 mg). The mixtures were analyzed by HPLC at 1 and 18 h.

2.6. Biological evaluation of technetium complexes

2.6.1. Cell growth

Human K-562 erythroleukemia cells [72] were seeded in suspension culture at a concentration of 2–3 × 10^5 cells/mL in RPMI-1640 (Gibco–Invitrogen, Life Technologies, Inc., U.S.A.) supplemented with 10% *v*/*v* FBS, streptomycin (1 μg/mL) and penicillin (1 U/mL) and maintained in exponential growth at 37 °C, in 5% CO_2 humidified atmosphere. Cell

number was determined by using a Neubauer hematocytometer under a light microscope.

2.6.2. Cell uptake studies

Exponentially grown K-562 cells (total number ~5×10^6) were incubated with ^{99m}Tc complex (40 μL, 2 MBq) for 15 and 30 min, as well as for 1, 2, 3, 4 and 18 h at 37 °C in an atmosphere containing 5% CO_2. After treatment, cells were collected, washed with 1× PBS twice and harvested with hypotonic buffer [10 mM Hepes, pH 7.9, 1.5 mM $MgCl_2$, 0.1 mM EDTA, 10 mM KCl, 0.5 mM dithiothreitol (DTT), supplemented with 1/100 Protease Inhibitor cocktail solution (Sigma, Aldrich)]. At this point the radioactivity of the cells was counted in γ-counter to evaluate the cellular uptake. The suspension was sonicated in an ultrasonic waterbath (Bandelin, Sonorex) for 20 min, followed by centrifugation (1000 *g*, 10 min) and the supernatant was collected as a cytosolic fraction A. Pellet A was harvested once again with same hypotonic buffer and cytosolic fraction B were separated from pellet B. The two cytosolic fractions (A and B) were further centrifuged (10,000 *g*, 10 min), with the supernatant collected as the cytosolic fraction C, while the resulting pellet C contained the mitochondria. Pellet B was resuspended in ~1 mL of high salt buffer (20 mM Hepes, pH 7.9, 1.5 mM $MgCl_2$, 0.2 mM EDTA, 0.42 M NaCl, 25% glycerol, 0.5 mM DTT, supplemented with 1/100 Protease Inhibitor cocktail solution) followed by sonication in the ultrasonic waterbath for 20 min. The suspension was centrifuged (15,000 *g*, 30 min) and the supernatant D was collected as the nuclear fraction [73]. The activity of the supernatant fraction C (cytosol), the nuclear fraction D, pellet B (membranes) and pellet C (mitochondria) were counted in a γ-counter to calculate the cellular distribution. The experiment was conducted in triplicates for each time point. Results are displayed in Fig. 9.

2.6.3. Biodistribution studies in mice

The biodistribution experiments were approved by the Aristotle University Committee for Animal Experimentation, according to the EU guidelines. Ten-week-old male BALB/c mice, of approximately 25 g weight were injected intravenously, each with ~370 kBq of the purified ^{99m}Tc complex in 0.1 mL saline. Animals were euthanized at 5 min and 2 h *p.i* by cervical dislocation followed by blood withdrawal and cardiectomy. Organs and tissues of interest were excised rapidly, weighed, and their radioactivity was determined using a gamma scintillator. The activity of the tissue samples was decay-corrected and calibrated by comparing the counts in the tissue with the counts of a standard solution corresponding to 1% of the injected dose. Counts of the sample and calibration aliquots were measured in the gamma counter at the same time. The amount of activity in the selected tissues and organs is expressed as a percent of the injected dose per organ/tissue (% ID) or per gram tissue (% ID/g). Values are quoted as the mean ID % ± standard deviation (SD) of the four mice per group. Blood volume, muscle mass and bone mass were estimated at 7, 43 and 10% of body weight, respectively. Results are displayed in Fig. 10 and Table S1.

3. Results and discussion

3.1. Synthesis and spectroscopic study of rhenium complexes

The complexes of the $[Re(CO)_3]^+$ core with the quinolone ligands, oxolinic acid and enrofloxacin, were prepared by use of the $[Re(CO)_3(MeOH)_3]^+$ precursor in methanol. Efforts to synthesize complexes **Re1** and **Re2** were first made by using $[NEt_4]_2[Re(CO)_3Br_3]$ as precursor. However, after monitoring the reaction by HPLC, incomplete conversion of the precursor to the complex was observed. Consequently, removal of bromide from the precursor was undertaken, which resulted in significant increase of the yield [73]. Addition of one equivalent of base was essential for the reaction completion but also for efficient dissolution of the quinolone. **Re1** is soluble in DMSO and **Re2** is soluble in ethanol, methanol, dichloromethane and DMSO.

All the [2+1] complexes comprising the bidentate quinolone ligands and the monodentate triphenylphosphine or imidazole co-ligands were synthesized by the reaction of the precursor $[Re(CO)_3(MeOH)_3]^+$ with equimolar amounts of both the ligands (Scheme 1). Average to high yields were obtained in all cases.

The resultant complexes are neutral, stable in the air and soluble in DMSO, but insoluble in most organic solvents and H_2O. The complexes possess a 1:1:1 Re:quinolone:L composition (L = MeOH, im, PPh_3), as it is indicated from elemental analysis. The values of the molar conductivity (Λ_M) of 1 mM DMSO solution of the complexes are within the range 5–12 $Scm^2\ mol^{-1}$ and might suggest a slightly partial ionization or a non-dissociation. Since for a 1:1 electrolyte, the Λ_M value should be ~70 $Scm^2\ mol^{-1}$, we may consider that the compounds do not dissociate in DMSO solution [30]. The complexes were characterized by elemental analysis, IR, NMR and UV–vis spectroscopic techniques and by X-ray crystallography.

The identity of the rhenium complexes, **Re1–Re5** was further corroborated by the presence of the *fac*-$[Re(CO)_3]$ core, as confirmed by IR spectroscopy. The characteristic stretching bands of the three coordinated C≡O ligands were observed at 2014–2021 cm^{-1}, 1879–1918 cm^{-1} and 1860–1889 cm^{-1} and fall in the same range as other *fac*-$[Re(CO)_3(O,O)]$ complexes [74–76].

The deprotonation and binding mode of the quinolones oxolinic acid and enrofloxacin was confirmed by IR spectroscopy. The band attributed to the ν(O–H) located at 3442(br(broad), m(medium)) cm^{-1} and 3443 (br,m) cm^{-1} for free Herx and Hoxo, respectively, has disappeared in the spectra of the complexes, indicating, thus, the deprotonation of the quinolone ligand. Additionally, the bands attributed to the $\nu(CO)_{carboxyl}$ and $\nu(C–O)_{carboxyl}$ stretching vibrations of the carboxylic group (−COOH) of the quinolones located at 1736(s(strong)) cm^{-1}

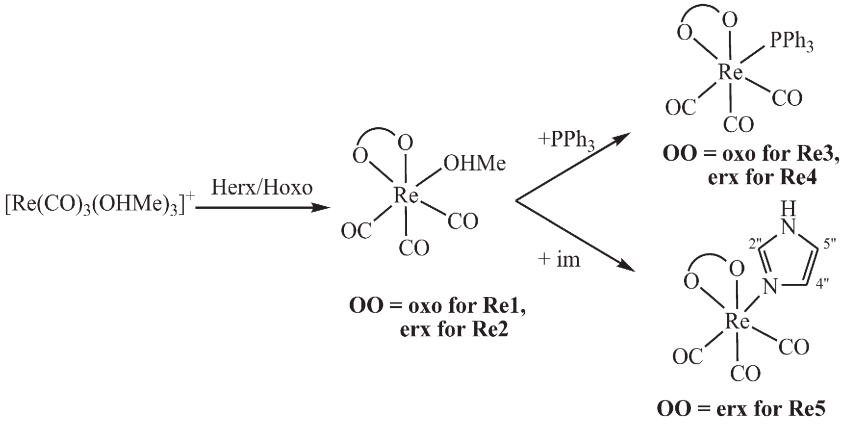

Scheme 1. Synthetic route for rhenium complexes **Re1–Re5**.

Table 2
Stability of rhenium complexes **Re1**–**Re5** studied by HPLC at room temperature for 0, 2, 24 and 72 h.

Complexes	t = 0 h	t = 2 h	t = 24 h	t = 72 h
Re1	92%	80%	48%	41%
Re2	100%	97%	95%	85%
Re3	100%	97%	85%	82%
Re4	100%	85%	80%	79%
Re5	95%	90%	87%	86%

and 1254(s) cm^{-1} and 1712(s) cm^{-1} and 1260(s) cm^{-1} for Herx and Hoxo, respectively, shifted in the range 1603–1618(vs) cm^{-1} and 1379–1400(m) cm^{-1} and were characterized as antisymmetric, $\nu_{asym}(CO_2)$, and symmetric, $\nu_{sym}(CO_2)$, stretching vibrations of the carboxylato group, respectively. The values of parameter $\Delta[=\nu_{asym}(CO_2) - \nu_{sym}(CO_2)]$ are in the range 203–239 cm^{-1} suggesting the monodentate coordination mode of the carboxylate group of the quinolone ligand [77]. The $\nu(CO)_{pyridone}$ stretching vibration of the quinolones at 1627 (vs(very strong)) cm^{-1} and 1633(s) cm^{-1} for Herx and Hoxo, respectively, shifted towards 1615(vs) cm^{-1} and 1644(vs) cm^{-1}, indicating the coordination of $O_{pyridone}$ to rhenium. All these spectral features are characteristic of binding of the deprotonated quinolone ligands to rhenium in a chelating bidentate mode via the pyridone oxygen and a carboxylato oxygen [16–18,26–30]. Furthermore, the characteristic bands of the triphenylphosphine ligand (748 cm^{-1} and 695 cm^{-1}) and the imidazole ligand (750 cm^{-1} and 659 cm^{-1}) were observed, confirming, thus, their coordination to rhenium [77].

The ^{1}H-NMR spectroscopy revealed the presence of the oxolinato and enrofloxacinato ligands in complexes **Re1** (Fig. S1) and **Re2**, respectively, as well as the presence of triphenylphosphine in **Re3** and **Re4** and imidazole in **Re5** (Fig. S2).

The stability of the rhenium complexes was tested in DMSO solution (≈1 mg/5 mL) over three days. Complexes **Re2**–**Re5** exhibited high stability (Table 2), while **Re1** decomposed significantly after 24 h (≈48% remained intact). Decomposition of the complexes was primarily attributed to re-oxidation of rhenium(I) to Re(VII), perrhenate, by the appearance of a relevant peak in the HPLC at 3 min.

3.2. Crystal structure of [Re(CO)$_3$(oxo)(PPh$_3$)]·0.5MeOH, *Re3*

A diagram of the structures of complex [Re(CO)$_3$(oxo)(PPh$_3$)] is depicted in Fig. 2, and selected bond distances and angles are listed in Table 3.

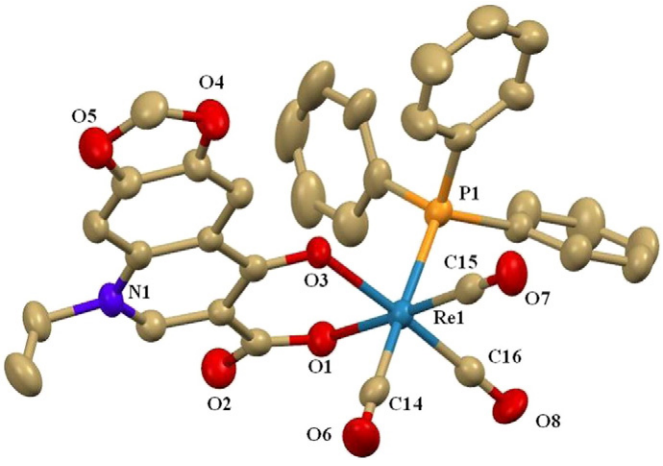

Fig. 2. A drawing of the molecular structure of [Re(CO)$_3$(oxo)(PPh$_3$)]. Hydrogen atoms are omitted for clarity.

Table 3
Selected bond distances (Å) and angles (°) for **Re3**.

Bond distance	(Å)	Bond distance	(Å)
Re(1)–O(1)	2.135(4)	Re(1)–C(14)	1.942(7)
Re(1)–O(3)	2.152(4)	Re(1)–C(15)	1.905(7)
Re(1)–P(1)	2.5008(16)	Re(1)–C(16)	1.908(6)
O(1)–C(1)	1.264(7)	O(2)–C(1)	1.234(7)
Bond angle	**(°)**	**Bond angle**	**(°)**
O(1)–Re(1)–O(3)	82.20(16)	O(3)–Re(1)–P(1)	89.10(12)
O(1)–Re(1)–P(1)	90.97(13)	O(3)–Re(1)–C(14)	90.4(2)
O(1)–Re(1)–C(14)	92.3(2)	O(3)–Re(1)–C(15)	96.0(2)
O(1)–Re(1)–C(15)	177.6(2)	O(3)–Re(1)–C(16)	176.5(2)
O(1)–Re(1)–C(16)	94.3(2)	C(14)–Re(1)–C(15)	89.3(3)
P(1)–Re(1)–C(14)	176.6(2)	C(14)–Re(1)–C(16)	89.4(3)
P(1)–Re(1)–C(15)	87.42(18)	C(15)–Re(1)–C(16)	87.5(3)
P(1)–Re(1)–C(16)	91.26(19)		

The complex is mononuclear and the oxolinato ligand behaves as deprotonated ligand in bidentate mode coordinated to rhenium via the pyridone oxygen O(3) and a carboxylato oxygen O(1) forming a six-membered chelate ring. In **Re3**, the rhenium atom is six-coordinated being in a distorted octahedral environment formed by two oxygen atoms (O(3) and O(1)) of the oxolinato ligand, a phosphorus atom (P(1)) of the triphenylphosphine ligand and three carbon atoms (C(14), C(15) and C(15)) from the carbonyl ligands. A solvate methanol is also present in the structure forming hydrogen-bonds with the non-coordinated carboxylato oxygen O(2) (H(354)…O(2) = 2.715 Å, O(9)…O(2) = 2.056 Å, O(9)–H(354)…O(2) = 137.2°).

A thorough search of the literature and the CCDC database concerning the rhenium complexes [Re(CO)$_3$(phosphine)(O,O′–ligand)] has revealed three different possibilities for the type the O,O′–ligand (i.e. the number n of the carbon atoms in–between the oxygen atoms as in –O– (C)$_n$–O–) (Scheme 2): (i) n = 1, i.e. –OCO– ligands (Scheme 2(A)), such as carboxylato–O,O′ ligands, forming a four-membered chelate ring with the distances around rhenium being in the range Re–O = 2.142–2.213 Å, Re–P = 2.414–2.496 Å and Re–C = 1.851–1.957 Å [78–82], (ii) n = 2, i.e. –O–C–C–O– ligands (Scheme 2(B)) (e.g. quinines, tropolonato or oxalato ligands) forming a five-membered chelate ring with the rhenium-distances being in the range Re–O = 2.125–2.181 Å, Re–P = 2.493–2.520 Å and Re–C = 1.891–1.959 Å [74,81–84] and (iii) n = 3, i.e. –O–C–C–C–O– ligands (acetylacetonato ligands and derivatives) (Scheme 2(C)) forming a six-membered chelate ring, as observed in complex **Re3**, with distances Re–O = 2.119–2.142 Å, Re–P = 2.464–2.498 Å and Re–C = 1.888–1.962 Å [75,76]. It is evident that the Re–C and Re–P distances are not closely related to the extent of the chelate ring, while the Re–O distances are shorter when more atoms are involved in the formation of the chelate ring. The Re–P (Re(1)–P(1) = 2.5008(16) Å) and Re–C (=1.905(7)–1.942(7) Å) distances in complex **Re3** are within the range expected for Re–P and Re–C, and the Re–O distances (Re(1)–O(3) = 2.152(4) Å and Re(1)–O(1) = 2.135(4) Å) are in the range observed for Re complexes of the third case (n = 3).

3.3. Interaction of the rhenium–quinolone complexes with CT DNA

The study of the interaction of quinolones and their complexes with DNA is of great interest due to the involvement of quinolones in the inhibition of DNA replication since their biological targets are DNA gyrase and topoisomerase IV [1–3]. The metal complexes of quinolones mainly interact with double-stranded DNA noncovalently, i.e. intercalation via π → π stacking interaction of the complex and DNA nucleobases, groove-binding due to van der Waals interaction or hydrogen-bonding or hydrophobic bonding, and the development of Coulomb forces to phosphate groups leading to electrostatic binding [85]. Several assays

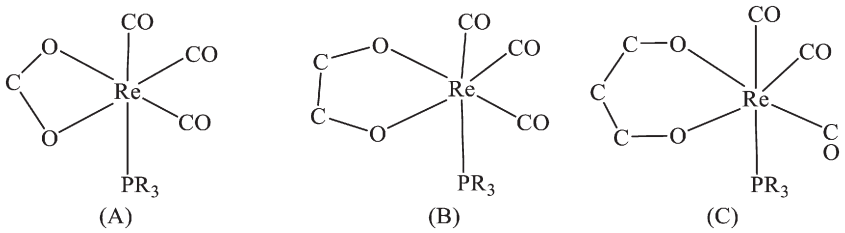

Scheme 2. The structural motifs of complexes [Re(CO)$_3$(phosphine)(O–(C)$_n$–O′–ligand)].

were performed in order to elucidate which of these types of noncovalent interaction may occur between the quinolones complexes and DNA.

In the UV spectra of the complexes in DMSO (2×10^{-5} M), the intense absorption bands observed are attributed to the intraligand transitions of the coordinated groups of enrofloxacinato and oxolinato ligands [29,33]. Any interaction between each complex and CT DNA may induce changes to the intraligand bands upon addition of CT DNA in diverse *r* values. The UV spectra of all complexes exhibited similar changes of the intraligand absorption band upon addition of a CT DNA solution, i.e. slight hypochromism up to 7% and no noteworthy shift of the λmax of the bands or, in few cases, a slight bathochromism (Table 4). The UV spectra of complexes **Re1** and **Re2** in DMSO (2×10^{-5} M) in the presence of increasing amounts of CT DNA are shown representatively in Fig. 3. In general, the existing results collected from the UV spectroscopic titration studies (slight hypochromism) are not elucidating concerning the DNA-interaction mode of the rhenium complexes and further experiments are necessary in order to clarify the binding mode [86].

The DNA-binding constants of the rhenium complexes (K_b) as calculated by the Wolfe–Shimer equation [67] (Eq. S1) and plots $^{[DNA]}/_{(\varepsilon_A-\varepsilon_f)}$ versus [DNA] (Fig. S3) are significantly higher than that of the corresponding free quinolone (Table 4) suggesting that its coordination to Re(I) results in a significant increase of the K_b value. The K_b values suggest a strong binding of the complexes to CT DNA and are similar or higher than that of the classical intercalator EB ($=1.23(\pm0.07) \times 10^5$ M^{-1}) as calculated in reference [87]. The K_b value of complex **Re2** ($=1.32(\pm0.03) \times 10^7$ M^{-1}) is among the highest DNA-binding constants reported for metal-quinolone complexes [11].

Viscosity measurements were carried out on CT DNA solutions (0.1 mM) upon addition of increasing amounts of the rhenium complexes (up to the value of r = 0.35). The relative DNA-viscosity (η/η_0) is sensitive to DNA-length (L/L_0) and they are related via the equation $L/L_0 = (\eta/\eta_0)^{1/3}$ [29]. Thus, important information concerning the DNA-interaction mode may be derived by studying the DNA-viscosity in the presence of a compound; when intercalation occurs, the DNA-bases are separated in order to host the intercalating compound leading to enhanced DNA-length and subsequently increase of the DNA-viscosity; in case of partial and/or non-classic intercalation (e.g. groove-binding or electrostatic interaction), the compounds do not enter in between the DNA-bases and a bend or a kink in the DNA helix may occur without affecting significantly the DNA-length and, thus, the DNA-viscosity may remain practically unchanged or even show a slight decrease. The relative DNA-viscosity exhibits a considerable increase in the presence of most complexes (Fig. 4). Such behavior may be attributed to the insertion of the complexes between the DNA-bases due to an intercalative interaction between DNA and each complex.

Table 4
Spectral features of the interaction of the rhenium complexes **Re1–Re5** with CT DNA. UV–band (λ in nm) (percentage of the observed hyper-/hypo-chromism (ΔA/A$_0$, %), blue-/red-shift of the λ$_{max}$ (Δλ, nm)), DNA-binding constants (K_b), percentage of EB–DNA fluorescence quenching (%ΔI/Io, %) and Stern–Volmer constants (K_{SV}).

Compound	Band (ΔA/A$_0$[a], Δλ[b])	K_b (M^{-1})	ΔI/I$_o$ (%)	K_{sv} (M^{-1})
Herx [18]	325 (+12[a], +3[b])	1.69×10^3	48.0	$1.91(\pm0.07) \times 10^5$
Hoxo [27]	324 (+50, −3[b]), 334 (+45, +4)	$3.02(\pm0.10) \times 10^3$	~0	nd[c]
Re1	307 (−7[a], +2)/337 (−2, 0)	$3.18(\pm0.12) \times 10^5$	75.1	$2.14(\pm0.05) \times 10^5$
Re2	342 (−4, 0)	$1.32(\pm0.03) \times 10^7$	82.1	$2.04(\pm0.08) \times 10^5$
Re3	338 (−2, 0)	$8.61(\pm0.14) \times 10^5$	68.0	$1.37(\pm0.06) \times 10^5$
Re4	341 (−1, 0)	$4.52(\pm0.24) \times 10^6$	86.0	$2.72(\pm0.15) \times 10^5$
Re5	343 (−1.5, 0)	$2.60(\pm0.14) \times 10^5$	68.8	$1.13(\pm0.04) \times 10^5$

[a] "+" denotes hyperchromism, "−" denotes hypochromism.
[b] "+" denotes red-shift, "−" denotes blue-shift.
[c] nd = not determined.

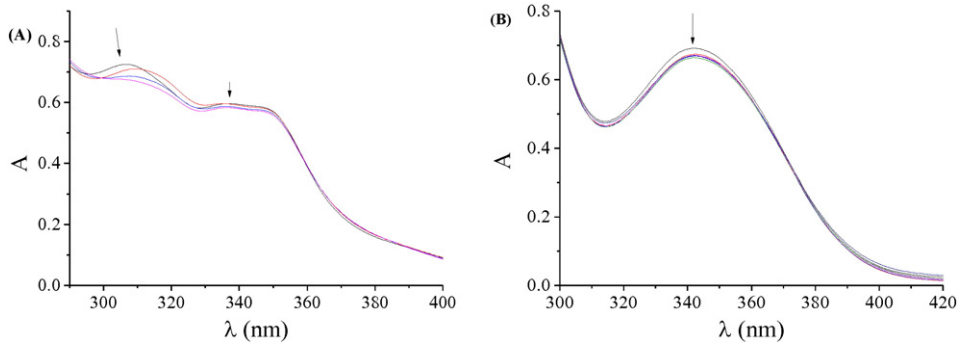

Fig. 3. UV spectra of DMSO solution (2×10^{-5} M) of complex (A) **Re1** and (B) **Re2** in the presence of increasing amounts of CT DNA ([DNA]/[complex] = 0–0.8). The arrows show the changes upon increasing amounts of CT DNA.

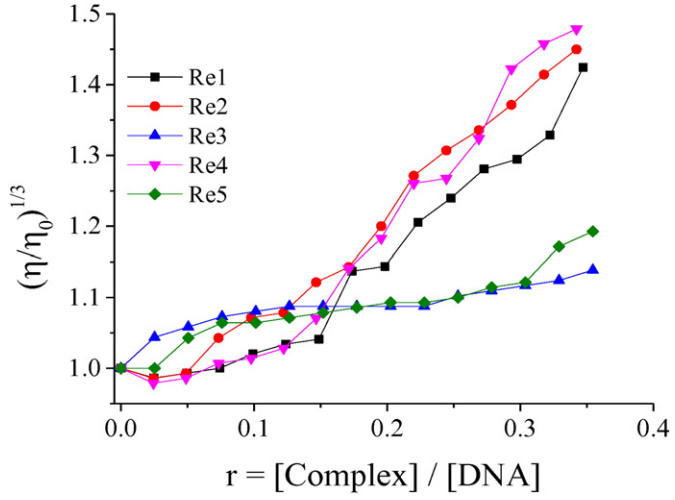

Fig. 4. Relative viscosity $(\eta/\eta_0)^{1/3}$ of CT DNA (0.1 mM) in buffer solution (150 mM NaCl and 15 mM trisodium citrate at pH 7.0) in the presence of complexes **Re1–Re5** at increasing amounts (r = [complex]/[DNA]).

The EB-displacing ability of the complexes from the EB–DNA complex may be considered a means to verify the existence of intercalation between the complexes and DNA. EB, as a fluorescence dye, is a typical indicator of intercalation, occurring via the insertion of the planar EB–phenanthridinium ring between adjacent base pairs on the double helix, since the EB–DNA complex emits intense fluorescence at 592 nm (with λ_{exit} = 540 nm) which may be quenched in the presence of a DNA-intercalating compound which competes with EB for the DNA-intercalating sites [88]. The rhenium complexes did not show any significant fluorescence at room temperature in solution or in the presence of CT DNA or EB upon excitation at 540 nm. Thus, the changes in the fluorescence emission spectra of a EB–DNA solution upon addition of the complexes can be used in order to investigate whether the complexes can displace EB from the EB–DNA complex.

The fluorescence emission spectra of pre-treated EB–CT DNA in the absence and presence of each complex were recorded for [EB] = 20 μM, [DNA] = 26 μM and for increasing amounts of the complex up to the value of r = 0.28 (shown representatively in Fig. 5(A) for **Re3**). The addition of the rhenium complexes at increasing amounts resulted in a moderate to significant decrease of the intensity of the emission band of the DNA–EB system at 592 nm (the final fluorescence is up to 14–32% of the initial EB–DNA fluorescence intensity in the presence of the complexes, Table 4) exhibiting the competition of the complexes with EB in binding to DNA (Fig. 5(B)) and their EB-displacing ability, proving thus indirectly their interaction with CT DNA via intercalation [29].

The Stern–Volmer plots of EB–DNA fluorescence studies in presence of the compounds (Fig. S4) show that the quenching of EB–DNA by the compounds is in good agreement (R = 0.99) with the linear Stern–Volmer equation (Eq. S2) proving the displacement of EB from EB–DNA by each compound [29]. The obtained values of K_{SV} (Table 4) are in the region reported for other metal-quinolone complexes [11] and may show tight binding of the complexes to DNA.

3.4. Binding of the rhenium–quinolone complexes to serum albumins

Albumins (SAs) are serum proteins responsible for the binding of ions and drugs and their transportation to cells and tissues through the bloodstream [69]. Since SAs are the most abundant plasma proteins, it is important to investigate their interaction with potent biological compounds (such as complexes **Re1–Re5**) as a preliminary step to monitor their potential transport towards their targets in the body [89] since such binding may lead to alternative transport pathways or changes of the biological properties of the compound. Human SA (HSA, having a tryptophan at position 214, i.e. Trp–214) and its homologue bovine SA (BSA, with two tryptophans Trp-134 and Trp-212) exhibit in solution noteworthy fluorescence emission at $\lambda_{em,max}$ = 351 nm and 343 nm, respectively, when excited at 295 nm, due to the tryptophan residues [69]. The inner-filter effect was not significant, as calculated with Eq. S3 [70], and did not affect the measurements.

The fluorescence emission band of HSA and BSA at $\lambda_{em,max}$ = 351 nm and 343 nm, respectively, exhibited in the presence of the rhenium complexes a low (for the oxolinato complexes) to moderate (for the enrfloxacinato complexes) quenching which was much more pronounced in the case of BSA (Fig. 6). Such quenching of the SA fluorescence emission may be attributed to possible changes in tryptophan environment of the SA due to changes in albumin secondary structure, indicating, thus, indirectly the binding of each compound to SA [90].

The quenching constants (k_q) for the interaction of complexes **Re1–Re5** with the SAs were calculated from the corresponding Stern–Volmer plots (Figs. S5 and S6) and the Stern–Volmer quenching equation (Eqs. S4 and S5). These values (Tables 4) suggest the significant ability of the complexes to quench the SA fluorescence via a static quenching mechanism [91], since the k_q are higher than 10^{12} M^{-1} s^{-1}. The k_q values of the complexes are in most cases similar or higher than those of corresponding free quinolone, with the enrofloxacinato complexes **Re4** and **Re2** having the highest k_q values for BSA and HSA, respectively ($k_{q(BSA),\mathbf{Re4}}$ = 2.22(±0.17)×10^{13} M^{-1} s^{-1} and $k_{q(BSA),\mathbf{Re2}}$ = 1.58(±0.24)×10^{13} M^{-1} s^{-1}) (Table 5). The values of the quenching constants

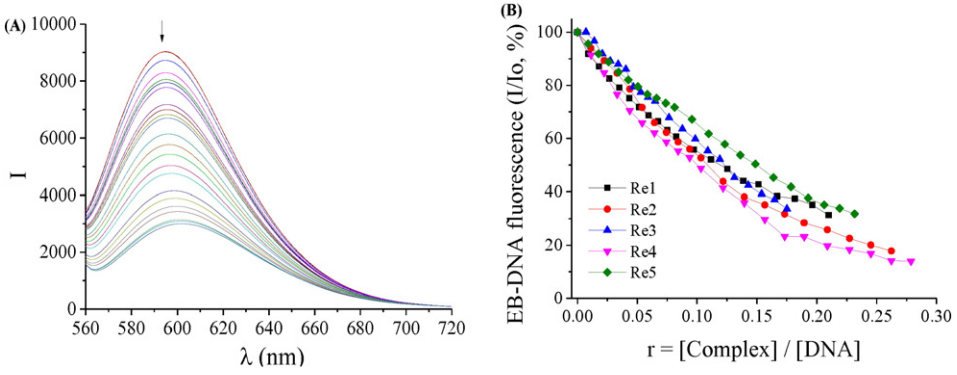

Fig. 5. (A) Emission spectra (λ_{exit} = 540 nm) for EB–DNA ([EB] = 20 μM, [DNA] = 26 μM) in buffer solution in the absence and presence of increasing amounts of complex **Re3** (up to the value of r = 0.18). The arrow shows the changes of intensity upon increasing amounts of **Re3.** (B) Plot of EB relative fluorescence intensity at λ_{em} = 592 nm (%) vs r (r = [complex]/[DNA]) (150 mM NaCl and 15 mM trisodium citrate at pH = 7.0) in the presence of complexes **Re1–Re5** (up to 24.9% of the initial EB–DNA fluorescence intensity for **Re1**, 17.9% for **Re2**, 32.0% for **Re3**, 14.0% for **Re4** and 31.2% for **Re5**).

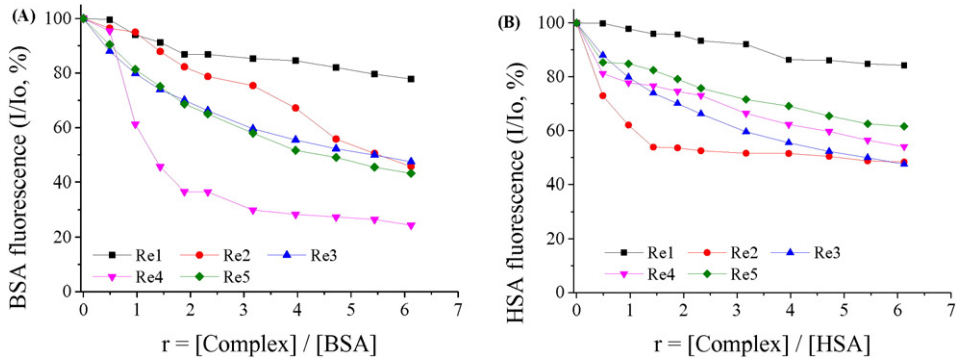

Fig. 6. (A) Plot of % relative fluorescence intensity at $\lambda_{em} = 343$ nm (%) vs r (r = [complex]/[BSA]) for the rhenium complexes (up to 77.8% of the initial BSA fluorescence for **Re1**, 45.7% for **Re2**, 47.5% for **Re3**, 24.4% for **Re4** and 43.3% for **Re5**) in buffer solution (150 mM NaCl and 15 mM trisodium citrate at pH 7.0). (B) Plot of % relative fluorescence intensity at $\lambda_{em} = 351$ nm (%) vs r (r = [complex]/[HSA]) for the rhenium complexes (up to 84.3% of the initial HSA fluorescence for **Re1**, 48.3% for **Re2**, 47.5% for **Re3**, 54.1% for **Re4** and 51.5% for **Re5**) in buffer solution (150 mM NaCl and 15 mM trisodium citrate at pH 7.0).

Table 5
The albumin quenching (k_q) and binding constants for the rhenium complexes **Re1**–**Re5**.

Compound	$k_{q\ (BSA)}$, ($M^{-1}\ s^{-1}$)	$K_{(BSA)}$, (M^{-1})	$k_{q(HSA)}$, ($M^{-1}\ s^{-1}$)	$K_{(HSA)}$, (M^{-1})
Herx [17]	4.40×10^{12}	1.82×10^{4}	3.56×10^{14}	7.63×10^{4}
Hoxo [18]	5.01×10^{12}	1.09×10^{5}	6.39×10^{12}	1.13×10^{5}
Re1	$1.44(\pm 0.09) \times 10^{12}$	$5.70(\pm 0.49) \times 10^{4}$	$1.11(\pm 0.04) \times 10^{12}$	$1.10(\pm 0.42) \times 10^{5}$
Re2	$6.61(\pm 0.36) \times 10^{12}$	$3.35(\pm 0.15) \times 10^{3}$	$1.58(\pm 0.24) \times 10^{13}$	$6.41(\pm 0.46) \times 10^{5}$
Re3	$1.72(\pm 0.03) \times 10^{13}$	$2.13(\pm 0.10) \times 10^{5}$	$5.89(\pm 0.20) \times 10^{12}$	$1.28(\pm 0.04) \times 10^{5}$
Re4	$2.22(\pm 0.17) \times 10^{13}$	$4.04(\pm 0.28) \times 10^{5}$	$4.08(\pm 0.24) \times 10^{12}$	$9.74(\pm 0.57) \times 10^{4}$
Re5	$7.24(\pm 0.14) \times 10^{12}$	$8.60(\pm 0.30) \times 10^{4}$	$3.26(\pm 0.17) \times 10^{12}$	$9.31(\pm 0.49) \times 10^{4}$

of the complexes are in the range found for a series of metal-complexes bearing quinolones as ligands [11].

The SA-binding constants of the complexes (K) were calculated from the corresponding Scatchard plots (Figs. S7 and S8) using the Scatchard equation (Eq. S6). The K values of the complexes (Table 5) are similar or higher than those of the corresponding free quinolone with complex **Re4** bearing the highest BSA-binding constant ($K_{(BSA),\mathbf{Re4}} = 4.04(\pm 0.28) \times 10^5\ M^{-1}$) and complex **Re2** having the highest HSA-binding constant ($K_{(HSA),\mathbf{Re2}} = 6.41(\pm 0.46) \times 10^5\ M^{-1}$). Furthermore, the K values of the complexes are of the same magnitude with those reported for a series of metal-quinolone complexes [11]. Regarding the stronger binding of complexes **Re3** and **Re4** with BSA as indicated by the higher k_q and K values, it is expected that the triphenylphosphine co-ligand increases the lipophilicity of the complexes, which is a known factor that increases SA binding [92].

Since the SA-binding constants of the rhenium complexes are in the range 3.35×10^3 – $6.41 \times 10^5\ M^{-1}$, we may consider them high enough so that the complexes bind to SAs and get transported to their biological targets. The complexes may have also the potential of being released upon arrival at their targets [90], since the derived SA-binding constants of the complexes are quite lower than the binding constant of diverse compounds to avidin ($K \approx 10^{15}\ M^{-1}$, such interactions are among the strongest known non-covalent ones [93]).

3.5. Topoisomerase IIα inhibition of *Re5*

We evaluated the Topo IIα inhibition activity of enrofloxacin and $[Re(CO)_3(erx)(im)]$ (**Re5**) via a DNA relaxation assay. Etoposide, a well-known enzyme inhibitor, was used as a positive control of the assay, and DMSO was also evaluated to discard its influence on the possible activity of the compounds. As can be seen in Fig. 7, Topo IIα activity (lanes 4 and 13) is readily detected by the presence of several relaxed DNA isoforms, topoisomers, migrating closely together. DMSO, at the concentration tested, does not affect enzymatic activity, while, as expected, etoposide acts as an interfacial poison, leading to the appearance of double stands breaks, and of the linear form of plasmid DNA.

The ligand Herx does not seem to inhibit the enzyme, at all concentrations tested. In contrast, complex **Re5** displayed a high to moderate ability of inhibiting Topo IIα at a concentration of 100 μM, but not at lower concentrations. This appreciably higher inhibition ability of complex **Re5** in comparison with the ligand seems to indicate that the metal coordination has a considerable impact on the biological activity of these compounds. The results of the present study suggest that Topo IIα could be an additional target for this family of Re tricarbonyl complexes.

3.6. Synthesis and biological evaluation of radiotracer $[^{99m}Tc(CO)_3(erx)(im)]$

3.6.1. Radiochemistry

The synthesis of $[^{99m}Tc(CO)_3(erx)(im)]$ was accomplished by heating the precursor $[^{99m}Tc(CO)_3(H_2O)_3]^{+1}$ with Herx, followed by the addition of imidazole (Scheme 3). Both ligands were added in 0.01 M concentration. Relatively high yield (≈75%) was obtained. The

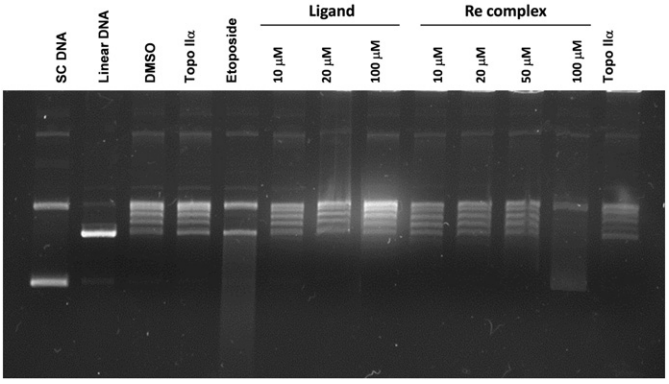

Fig. 7. Topo IIα inhibition capacity of enrofloxacin (L) and complex **Re5**, determined by a DNA relaxation assay. Supercoiled and linear DNA were used as references (lanes 1 and 2, respectively). Relaxed DNA bands (lane 4) show an intact Topo IIα activity.

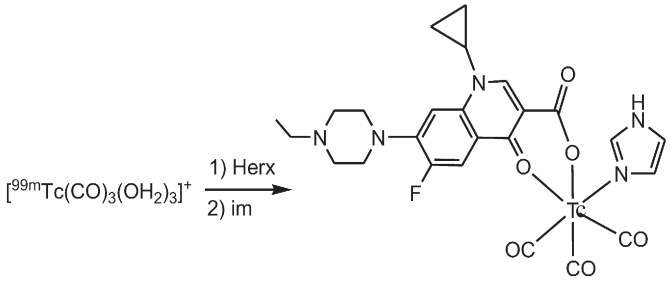

Scheme 3. Synthesis of complex [^{99m}Tc(CO)$_3$(erx)(im)].

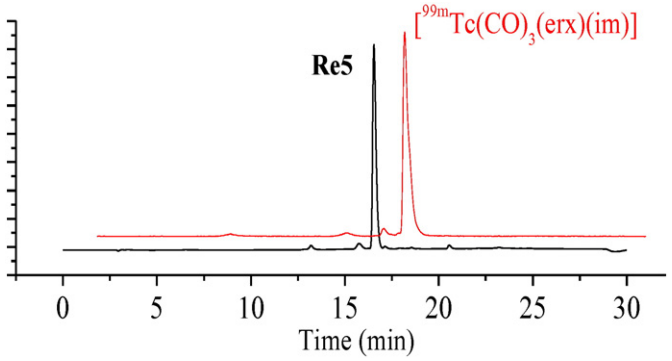

Fig. 8. Comparative HPLC analysis of [Re(CO)$_3$(erx)(im)], t_R = 17.0 min (front trace, black line) and [^{99m}Tc(CO)$_3$(erx)(im)], t_R = 17.1 min (back trace, red line).

conditions employed for the radiolabeling were similar to the ones used in the radiolabeling of other quinolones [94,95]. The ^{99m}Tc complex was purified by HPLC and, then, its identification was accomplished by comparative HPLC analysis, using its rhenium analogue **Re5** as standard (Fig. 8). Rhenium is considered as surrogate metal to technetium, due to their chemical and physical similarities and they often form analogous complexes with almost identical retention times in the HPLC. The stability of the ^{99m}Tc tracer in phosphate buffer solution (PBS) over 18 h was very high (90%).

3.6.2. Cell uptake studies

Incubation of the tracer ^{99m}Tc complex [^{99m}Tc(CO)$_3$(erx)(im)] with K-562 erythroleukemia cells over 20 h led to a time-dependent uptake of the complex at approximately 1.4% of the initial dose (Fig. 9(A)). Subsequent lysis of the cells and isolation of the mitochondrial, nuclear and cytosolic fractions indicated that the radioactivity had been distributed in all these three cellular compartments, while low percentage of the radioactivity measured corresponded to binding on the membrane (pellet B). The distribution of the radioactivity in the cellular compartments overtime showed an increased accumulation in the mitochondria that reached ≈40% at 20 h (Fig. 9(B)).

3.6.3. Biodistribution studies

The biodistribution of tracer complex [^{99m}Tc(CO)$_3$(erx)(im)] in healthy mice after intravenous administration showed fast clearance from blood and muscle (Fig. 10). In addition, significant renal excretion was observed, where 26.38 ± 7.39% injected dose (ID) is in the kidneys at 5 min *p.i.* that drops to 6.3 5 ± 0.67% after 2 h, while 44.40 ± 6.06% of the injected dose is excreted in the urine after 2 h. Similarly, high initial liver uptake (35.76 ± 5.86% ID, at 5 min *p.i.*) is followed by hepatobiliary excretion, 30.07 ± 3.79% I.D. after 2 h (Table S1). These pharmacokinetic characteristics show a potential for the use of this type of quinolone [2 + 1] complexes as imaging agents.

4. Conclusions

The synthesis and characterization of the mononuclear rhenium(I) tricarbonyl complexes with the quinolones oxolinic acid and enrofloxacin in the presence of the O-donor ligand methanol, the P-donor ligand triphenylphosphine or the N-donor ligand imidazole was successfully achieved. In the complexes, the quinolone ligands are deprotonated being bidentately coordinated to rhenium via the pyridone and a carboxylate oxygen. The crystal structure of complex [Re(CO)$_3$(oxo)(PPh$_3$)]·0.5MeOH was determined by X-ray crystallography revealing a octahedral geometry for Re(I) and is the first crystal structure of a Re(I)–quinolone complex.

UV spectroscopy studies and viscosity measurements revealed the ability of the complexes to bind to CT DNA possibly be intercalation. The complex [Re(CO)$_3$(erx)(MeOH)] exhibits the highest DNA-binding constant (K_b = 1.32(±0.03)×10^7 M^{-1}), among the complexes examined, which is higher than the K_b value of the classic intercalator EB as calculated in our lab and among the highest metal-quinolone complexes. Competitive binding studies with EB revealed the EB-displacing ability of the complexes from the EB–CT DNA complex, confirming, thus, indirectly that intercalation may be the most possible DNA-interaction mode, a conclusion lying in accordance to the viscometry interaction studies.

In addition, enhanced inhibitory topoisomerase IIα activity for the [2 + 1] complex [Re(CO)$_3$(erx)(im)] was observed, in comparison to free enrofloxacin. Therefore, the *in vitro* studies of the rhenium complexes with DNA and with the DNA enzyme topoisomerase IIα indicate that the coordination of quinolones with the Re-tricarbonyl core leads to complexes with enhanced activity towards these biological targets. Furthermore, the interaction of rhenium complexes with bovine or human serum albumins was investigated by fluorescence emission spectroscopy revealing the binding to BSA and HSA with relatively

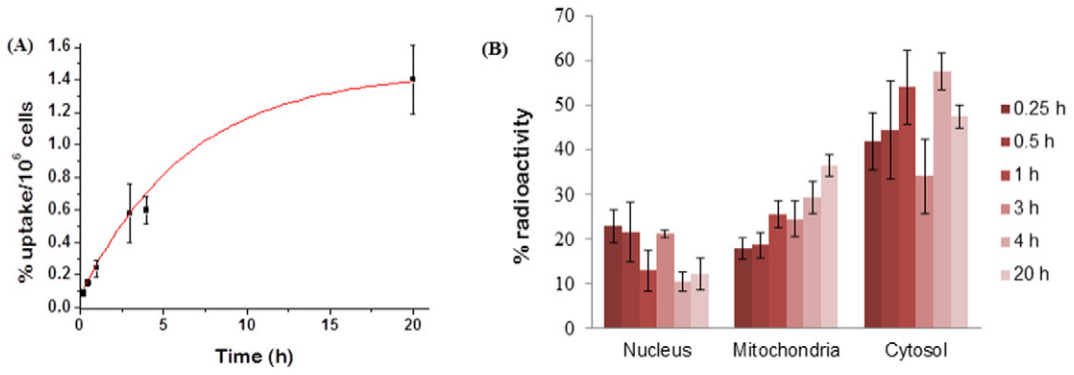

Fig. 9. (A) Uptake curve of [^{99m}Tc(CO)$_3$(erx)(im)] in K-562 cells for a time period of 20 h. Each time point represents mean value ± SD of three independent cultures. (B) Cellular distribution of [^{99m}Tc(CO)$_3$(erx)(im)] in K-562 cells at various time points (mean value ± SD) from triplicates experiments).

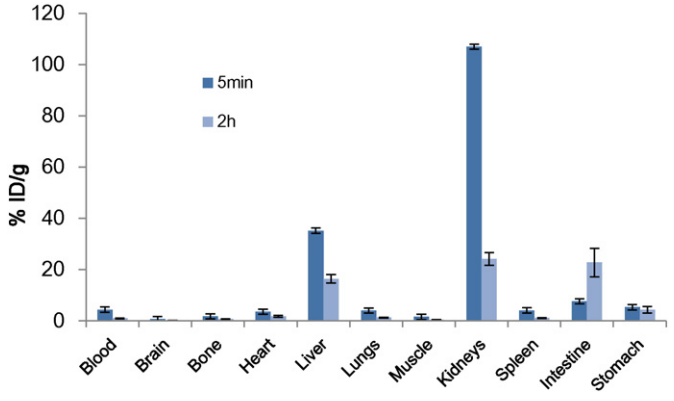

Fig. 10. Biodistribution of [^{99m}Tc(CO)$_3$(erx)(im)] in healthy mice, expressed as % injected dose/g tissue (mean value ± SD, n = 4).

high binding constants (K = 3.35×10^3 – 6.41×10^5 M^{-1}); these values may be considered as lying in an optimum range to suggest binding, transfer and release upon arrival at their targets.

The tracer complex [^{99m}Tc(CO)$_3$(erx)(im)] was prepared in high yield and was found able to enter K-562 human erythroleukemia cells. The majority of the radioactivity was found in the cytoplasm and the mitochondrial fraction, while a lower nuclear uptake was also observed. A tendency for accumulation of the radioactivity in the mitochondria makes the complex interesting for further evaluation. Overall, these results indicate that the distribution of this type of ^{99m}Tc tracers may be related to binding to intracellular targets such as mitochondrial DNA or the DNA-topoisomerase complex. In addition, the biodistribution results indicate that the [2 + 1] ^{99m}Tc-tricarbonyl quinolone complexes show a suitable pharmacokinetic profile for further evaluation as imaging agents in future studies.

Abbreviations

br	broad
BSA	bovine serum albumin
CT	calf-thymus
DMF	N,N-dimethylformamide
DTT	dithiothreitol
EB	ethidium bromide, 3,8-diamino-5-ethyl-6-phenyl-phenanthridinium bromide
erx	enrofloxacinato
Hepes	4-(2-hydroxyethyl)-1-piperazineethanesulfonic acid
Herx	enrofloxacin, 1-cyclopropyl-7-(4-ethyl-piperazin-1-yl)-6-fluoro-4-oxo-1,4-dihydro-quinoline-3-carboxylic acid
Hoxo	oxolinic acid, 5,8-dihydro-5-ethyl-8-oxo-1,3-dioxolo[4,5-g]quinoline-7-carboxylic acid
HSA	human serum albumin
ID	injected dose
im	imidazole
K	SA-binding constant
K_b	DNA-binding constant
k_q	quenching constant
K_{SV}	Stern–Volmer constant
m	medium
oxo	oxolinato
PBS	Phosphate-buffered saline
PPh_3	triphenylphosphine
r	[complex]/[DNA] ratio
r'	[DNA]/[complex] ratio
s	strong
SA	serum albumin
SDS	Sodium dodecyl sulfate
sh	shoulder
SPECT	Single Photon Emission Computed Tomography
t_R	HPLC retention time
vs	very strong
Δ	$\nu_{asym}(CO_2) - \nu_{sym}(CO_2)$

Acknowledgement

This research project was supported by EU COST Action CM1105: "Functional metal complexes that bind to biomolecules". The authors would like to acknowledge FCT, Portugal for financial support (project C^{2}TN — UID/Multi/04349/2013 and FCT Investigator Grant to F. Mendes).

Appendix A. Supplementary data

CCDC 1427952 contains the supplementary crystallographic data for this paper. These data can be obtained free of charge via www.ccdc.cam.ac.uk/conts/retrieving.html (or from the Cambridge Crystallographic Data Centre, 12 Union Road, Cambridge CB21EZ, UK; fax: (+44) 1223–336–033; or deposit@ccde.cam.ac.uk). Supplementary data associated with this article can be found, in the online version, at http://dx.doi.org/10.1016/j.jinorgbio.2015.12.010.

References

[1] V.T. Andriole (Ed.), The Quinolones, Academic Press, 2000.
[2] D.E. King, R. Malone, S.H. Lilley, Am. Fam. Physician 61 (2000) 2741–2748.
[3] I. Turel, Coord. Chem. Rev. 232 (2002) 27–47.
[4] N. Ahmed, M. Dawson, C. Smith, E. Wood, Biology of Diesease, Taylor & Francis, 2007 41–71 (ch. 3).
[5] J. Tuma, W.H. Connors, D.H. Stitelman, C. Richert, J. Am. Chem. Soc. 124 (2002) 4236–4246.
[6] K. Sandstrom, S. Warmlander, M. Leijon, A. Graslund, Biochem. Biophys. Res. Commun. 304 (2003) 55–59.
[7] S.H. Elsea, M. Westergaard, D.A. Burden, J.P. Lomenick, N. Osheroff, Biochemistry 36 (1997) 2919–2924.
[8] V.E. Anderson, N. Osheroff, Curr. Pharm. Des. 7 (2001) 339–355.
[9] F. Arjmand, I. Yousuf, T. Ben Hadda, L. Toupet, Eur. J. Med. Chem. 81 (2014) 76–88.
[10] L.R. Gouvea, L.S. Garcia, D.R. Lachter, P.R. Nunes, F. de Castro Pereira, E.P. Silveira-Lacerda, S.R.W. Louro, P.J.S. Barbeira, L.R. Teixeira, Eur. J. Med. Chem. 55 (2012) 67–73.
[11] G. Psomas, D.P. Kessissoglou, Dalton Trans. 42 (2013) 6252–6276.
[12] N. Jimenez–Garrido, L. Perello, R. Ortiz, G. Alzuet, M. Gonzalez–Alvarez, E. Canton, M. Liu–Gonzalez, S. Garcia–Granda, M. Perez–Priede, J. Inorg. Biochem. 99 (2005) 677–689.
[13] P. Drevensek, T. Zupancic, B. Pihlar, R. Jerala, U. Kolitsch, A. Plaper, I. Turel, J. Inorg. Biochem. 99 (2005) 432–442.
[14] I. Turel, J. Kljun, F. Perdih, E. Morozova, V. Bakulev, N. Kasyanenko, J.A.W. Byl, N. Osheroff, Inorg. Chem. 49 (2010) 10750–10752.
[15] Y. Wang, R. Hu, D. Jiang, P. Zhang, Q. Lin, Y. Wang, J. Fluoresc. 21 (2011) 813–832.
[16] K.C. Skyrianou, F. Perdih, I. Turel, D.P. Kessissoglou, G. Psomas, J. Inorg. Biochem. 104 (2010) 161–170.
[17] K.C. Skyrianou, V. Psycharis, C.P. Raptopoulou, D.P. Kessissoglou, G. Psomas, J. Inorg. Biochem. 105 (2011) 63–74.
[18] A. Tarushi, C.P. Raptopoulou, V. Psycharis, A. Terzis, G. Psomas, D.P. Kessissoglou, Bioorg. Med. Chem. 18 (2010) 2678–2685.
[19] V. Uivarosi, Molecules 18 (2013) 11153–11197.
[20] I. Turel, A. Golobic, A. Klavzar, B. Pihlar, P. Buglyo, E. Tolis, D. Rehder, K. Sepcic, J. Inorg. Biochem. 95 (2003) 199–207.
[21] M.P. Lopez–Gresa, R. Ortiz, L. Perello, J. Latorre, M. Liu–Gonzalez, S. Garcia–Granda, M. Perez–Priede, E. Canton, J. Inorg. Biochem. 92 (2002) 65–74.
[22] C. Protogeraki, E.G. Andreadou, F. Perdih, I. Turel, A.A. Pantazaki, G. Psomas, Eur. J. Med. Chem. 86 (2014) 189–201.
[23] E.K. Efthimiadou, H. Thomadaki, Y. Sanakis, C.P. Raptopoulou, N. Katsaros, A. Scorilas, A. Karaliota, G. Psomas, J. Inorg. Biochem. 101 (2007) 64–73.
[24] M.E. Katsarou, E.K. Efthimiadou, G. Psomas, A. Karaliota, D. Vourloumis, J. Med. Chem. 51 (2008) 470–478.
[25] D.J. D'Alessio, V.M. Olexy, G.G. Jackson, Antimicrob. Agents Chemother. 7 (1967) 490–496.
[26] G. Psomas, A. Tarushi, E.K. Efthimiadou, Y. Sanakis, C.P. Raptopoulou, N. Katsaros, J. Inorg. Biochem. 100 (2006) 1764–1773.
[27] A. Tarushi, G. Psomas, C.P. Raptopoulou, D.P. Kessissoglou, J. Inorg. Biochem. 103 (2009) 898–905.
[28] A. Tarushi, K. Lafazanis, J. Kljun, I. Turel, A.A. Pantazaki, G. Psomas, D.P. Kessissoglou, J. Inorg. Biochem. 121 (2013) 53–65.
[29] M. Zampakou, M. Akrivou, E.G. Andreadou, C.P. Raptopoulou, V. Psycharis, A.A. Pantazaki, G. Psomas, J. Inorg. Biochem. 121 (2013) 88–99.
[30] E.P. Irgi, G.D. Geromichalos, S. Balala, J. Kljun, S. Kalogiannis, A. Papadopoulos, I. Turel, G. Psomas, RSC Adv. 5 (2015) 36353–36367.

[31] C.A. Rees, D.M. Boothe, J. Am. Vet. Med. Assoc. 224 (2004) 1455–1458.
[32] I. Turel, I. Leban, G. Klintschar, N. Bukovec, S. Zalar, J. Inorg. Biochem. 66 (1997) 77–82.
[33] A. Tarushi, G. Psomas, C.P. Raptopoulou, V. Psycharis, D.P. Kessissoglou, Polyhedron 28 (2009) 3272–3278.
[34] E.K. Efthimiadou, M. Katsarou, Y. Sanakis, C.P. Raptopoulou, A. Karaliota, N. Katsaros, G. Psomas, J. Inorg. Biochem. 100 (2006) 1378–1388.
[35] J. Recillas–Mota, M. Flores–Alamo, R. Moreno–Esparza, J. Gracia–Mora, Acta Crystallogr. E63 (2007) m3030–m3031.
[36] Z. An, J. Gao, W.T.A. Harrison, J. Coord. Chem. 63 (2010) 3871–3879.
[37] S.S. Jurisson, J.D. Lydon, Chem. Rev. 99 (1999) 2205–2218.
[38] M.D. Bartholoma, A.S. Louie, J.F. Valliant, J. Zubieta, Chem. Rev. 110 (2010) 2903–2920.
[39] S.E. Pool, E.P. Krenning, G. Koning, C.H.J. van Eijck, J.H.M. Teunissen, B. Kam, R. Valkema, D.J. Kwekkeboom, M. de Jong, Semin. Nucl. Med. 40 (2010) 209–218.
[40] M. De Jong, W.P. Breeman, D.J. Kwekkeboom, R. Valkema, E.P. Krenning, Acc. Chem. Res. 42 (2009) 873–880.
[41] Y. Zhou, S. Liu, Bioconjug. Chem. 22 (2011) 1459–1472.
[42] C. Moura, F. Mendes, L. Gano, I. Santos, A. Paulo, J. Inorg. Biochem. 123 (2013) 34–45.
[43] N. Agorastos, L. Borsig, A. Renard, P. Antoni, G. Viola, B. Spingler, P. Kurz, R. Alberto, Chem. Eur. J. 13 (2007) 3842–3852.
[44] K. Zelenka, L. Borsig, R. Alberto, Org. Biomol. Chem. 9 (2011) 1071–1078.
[45] R. Alberto, Top. Organomet. Chem. 32 (2010) 219–246.
[46] V. Vassiliadis, C. Triantis, C.P. Raptopoulou, V. Psycharis, A. Terzis, I. Pirmettis, M.S. Papadopoulos, D. Papagiannopoulou, Polyhedron 81 (2014) 511–516.
[47] P. Haefliger, N. Agorastos, A. Renard, G. Giambonini–Brugnoli, C. Marty, R. Alberto, Bioconjug. Chem. 16 (2005) 582–587.
[48] T. Esteves, F. Marques, A. Paulo, J. Rino, P. Nanda, C.J. Smith, I. Santos, J. Biol. Inorg. Chem. 16 (2011) 1141–1153.
[49] R.F. Vitor, I. Correia, M. Videira, F. Marques, A. Paulo, J. Costa Pessoa, G. Viola, G.G. Martins, I. Santos, Chembiochem 9 (2008) 131–142.
[50] A.V. Hall, K.K. Solanki, S. Vinjamuri, K.E. Britton, S.S. Das, J. Clin. Pathol. 51 (1998) 215–219.
[51] K.K. Halder, D.K. Nayak, R. Baishya, B.R. Sarkar, S. Sinha, S. Ganguly, M.C. Debnath, Metallomics 3 (2011) 1041–1048.
[52] S.Q. Shah, M.R. Khan, Appl. Radiat. Isot. 69 (2011) 686–690.
[53] A. Leonidova, G. Gasser, ACS Chem. Biol. 9 (2014) 2180–2193.
[54] A. Kastl, S. Dieckmann, K. Wähler, T. Völker, L. Kastl, A.L. Merkel, A. Vultur, B. Shannan, K. Harms, M. Ocker, W. Parak, M. Herlyn, E. Meggers, ChemMedChem 8 (2013) 924–927.
[55] K. Wähler, A. Ludewig, P. Szabo, K. Harms, E. Meggers, Eur. J. Inorg. Chem. 807–811 (2014).
[56] V. Fernandez-Moreira, F.L. Thorp-Greenwood, A.J. Amoroso, J. Cable, J.B. Court, V. Gray, A.J. Hayes, R.L. Jenkins, B.M. Kariuki, D. Lloyd, C.O. Millet, C.F. Williams, M.P. Coogan, Org. Biomol. Chem. 8 (2010) 3888–3901.
[57] R. Alberto, A. Egli, U. Abram, K. Hegetschweiler, V. Gramlich, P.A. Schubiger, J. Chem. Soc. Dalton Trans. (1994) 2815–2820.
[58] H. He, M. Lipowska, X. Xu, A.T. Taylor, M. Carlone, L.G. Marzilli, Inorg. Chem. 44 (2005) 5437–5446.
[59] R. Schibli, R. La Bella, R. Alberto, E. Garcia–Garayoa, K. Ortner, U. Abram, P.A. Schubiger, Bioconjug. Chem. 11 (2000) 345–351.
[60] J. Marmur, J. Mol. Biol. 3 (1961) 208–211.
[61] M.F. Reichmann, S.A. Rice, C.A. Thomas, P. Doty, J. Am. Chem. Soc. 76 (1954) 3047–3053.
[62] Bruker Analytical X–ray Systems, Inc., Apex2, version 2 user manual, M86–E01078, Madison, WI, 2006.
[63] Siemens Industrial Automation, Inc., SADABS: area-detector absorption correction, Madison, WI, 1996.
[64] L. Palatinus, G. Chapuis, J. Appl. Crystallogr. 40 (2007) 786.
[65] P.W. Betteridge, J.R. Carruthers, R.I. Cooper, K. Prout, D.J. Watkin, J. Appl. Crystallogr. 36 (2003) 1487.
[66] D.J. Watkin, C.K. Prout, L.J. Pearce, CAMERON Program, Chemical Crystallographic Laboratory, Oxford University, UK, 1996.
[67] A. Wolfe, G. Shimer, T. Meehan, Biochemistry 26 (1987) 6392–6396.
[68] G. Zhao, H. Lin, S. Zhu, H. Sun, Y. Chen, J. Inorg. Biochem. 70 (1998) 219–226.
[69] J.R. Lakowicz, Principles of Fluorescence Spectroscopy, third ed. Plenum Press, New York, 2006.
[70] L. Stella, A.L. Capodilupo, M. Bietti, Chem. Commun. (2008) 4744–4746.
[71] Y. Wang, H. Zhang, G. Zhang, W. Tao, S. Tang, J. Lumin. 126 (2007) 211–218.
[72] C.B. Lozzio, B.B. Lozzio, Blood 45 (1975) 321–334.
[73] E. Warabi, W. Takabe, T. Minami, K. Inoue, K. Itoh, M. Yamamoto, T. Ishii, T. Kodama, N. Noguchi, Free Radic. Biol. Med. 42 (2007) 260–269.
[74] M. Schutte, A. Roodt, H.G. Visser, Inorg. Chem. 51 (2012) 11996–12006.
[75] C. Triantis, T. Tsotakos, C. Tsoukalas, M. Sagnou, C. Raptopoulou, A. Terzis, V. Psycharis, M. Pelecanou, I. Pirmettis, M. Papadopoulos, Inorg. Chem. 52 (2013) 12995–13003.
[76] M. Sagnou, D. Benaki, C. Triantis, T. Tsotakos, V. Psycharis, C.P. Raptopoulou, I. Pirmettis, M. Papadopoulos, M. Pelecanou, Inorg. Chem. 50 (2011) 1295–1303.
[77] K. Nakamoto, Infrared and Raman Spectra of Inorganic and Coordination Compounds, Part B: Applications in Coordination, Organometallic, and Bioinorganic Chemistry, sixth ed. Wiley, New Jersey, 2009.
[78] D.H. Gibson, Y. Ding, R.L. Miller, B.A. Sleadd, M.S. Mashuta, J.F. Richardson, Polyhedron 18 (1999) 1189–1200.
[79] D.H. Gibson, J.M. Mehta, M. Ye, J.F. Richardson, M.S. Mashuta, Organometallics 13 (1994) 1070–1072.
[80] D.H. Gibson, M. Ye, J.F. Richardson, M.S. Mashuta, Organometallics 13 (1994) 4559–4569.
[81] R.I. Bochkova, L.N. Zakharov, N.V. Patrikeeva, K.G. Shalnova, G.A. Abakumov, V.K. Cherkasov, Koord. Khim. (Russ. Coord. Chem.), 13 (1987) 702.
[82] C.P. Cheng, S.R. Wang, J.C. Lin, S. Wang, J. Organomet. Chem. 249 (1988) 375–382.
[83] C.L. Kee, F. Zhou, H. Su, Y.K. Yan, J. Organomet. Chem. 792 (2015) 211–219.
[84] R. Zhang, C.L. Kee, W.K. Leong, Y.K. Yan, J. Organomet. Chem. 689 (2004) 2837–2844.
[85] E.C. Long, J.K. Barton, Acc. Chem. Res. 23 (1990) 271–273.
[86] G. Pratviel, J. Bernadou, B. Meunier, Adv. Inorg. Chem. 45 (1998) 251–262.
[87] A. Dimitrakopoulou, C. Dendrinou–Samara, A.A. Pantazaki, M. Alexiou, E. Nordlander, D.P. Kessissoglou, J. Inorg. Biochem. 102 (2008) 618–628.
[88] W.D. Wilson, L. Ratmeyer, M. Zhao, L. Strekowski, D. Boykin, Biochemistry 32 (1993) 4098–4104.
[89] C. Tan, J. Liu, H. Li, W. Zheng, S. Shi, L. Chen, L. Ji, J. Inorg. Biochem. 102 (2008) 347–358.
[90] V. Rajendiran, R. Karthik, M. Palaniandavar, H. StoeckliEvans, V.S. Periasamy, M.A. Akbarsha, B.S. Srinag, H. Krishnamurthy, Inorg. Chem. 46 (2007) 8208–8221.
[91] S. Wu, W. Yuan, H. Wang, Q. Zhang, M. Liu, K. Yu, J. Inorg. Biochem. 102 (2008) 2026–2034.
[92] G. Colmenarejo, A. Alvarez-Pedraglio, J. Lavandera, J. Med. Chem. 44 (2001) 4370–4378.
[93] O.H. Laitinen, V.P. Hytonen, H.R. Nordlund, M.S. Kulomaa, Cell. Mol. Life Sci. 63 (2006) 2992–3017.
[94] S.Q. Shah, M.R. Khan, J. Radioanal. Nucl. Chem. 288 (2011) 485–490.
[95] D.K. Nayak, R. Baishya, K.K. Halder, T. Sen, B.R. Sarkar, S. Ganguly, M.K. Das, M.C. Debnath, Metallomics 4 (2012) 1197–1208.